LANGMUIR Article
Cite This: Langmuir 2018, 34, 15526−15536
pubs.acs.org/Langmuir

Adsorption and Crystallization of Particles at the Air−Water Interface Induced by Minute Amounts of Surfactant

Manos Anyfantakis,*[,†,‡,#] Jacopo Vialetto,[†,#] Andreas Best,[§] Günter K. Auernhammer,[§,∥] Hans-Jürgen Butt,[§] Bernard P. Binks,[⊥] and Damien Baigl*[,†]

[†]PASTEUR, Department of Chemistry, École Normale Supérieure, PSL University, Sorbonne Université, CNRS, 75005 Paris, France

[‡]Physics & Materials Science Research Unit, University of Luxembourg, 162a Avenue de la Faiencerie, Luxembourg L-1511, Luxembourg

[§]Max Planck Institute for Polymer Research, Ackermannweg 10, 55128 Mainz, Germany

[∥]Leibniz Institute for Polymer Research, Hohe Straße 6, 01069 Dresden, Germany

[⊥]School of Mathematics and Physical Sciences, University of Hull, Hull HU6 7RX, U.K.

Supporting Information

ABSTRACT: Controlling the organization of particles at liquid−gas interfaces usually relies on multiphasic preparations and external applied forces. Here, we show that micromolar amounts of a conventional cationic surfactant induce, in a single step, both adsorption and crystallization of various types of nanometer- to micrometer-sized anionic particles at the air−water interface, without any additional phase involved or external forces other than gravity. Contrary to conventional surfactant-induced particle adsorption through neutralization and hydrophobization at a surfactant concentration close to the critical micellar concentration (CMC), we show that in our explored concentration regime (CMC/1000-CMC/100), particles adsorb with a low contact angle and maintain most of their charge, leading to the formation of two-dimensional assemblies with different structures, depending on surfactant (C_s) and particle (C_p) concentrations. At low C_s and C_p, particles are repulsive and form disordered assemblies. Increasing C_p in this regime increases the number of adsorbed particles, leading to the formation of mm-sized, highly ordered polycrystalline assemblies because of the long-range attraction mediated by the collective deformation of the interface. Increasing C_s decreases the particle repulsion and therefore the interparticle distance within the monocrystalline domains. A further increase in C_s (≈CMC/10) leads to a progressive neutralization of particles accompanied by the formation of disordered structures, ranging from densely packed amorphous ones to loosely packed gels. These results emphasize a new role of the surfactant to mediate both adsorption and crystallization of particles at liquid−gas interfaces and provide a practical manner to prepare two-dimensional ordered colloidal assemblies in a remarkably robust and convenient manner.

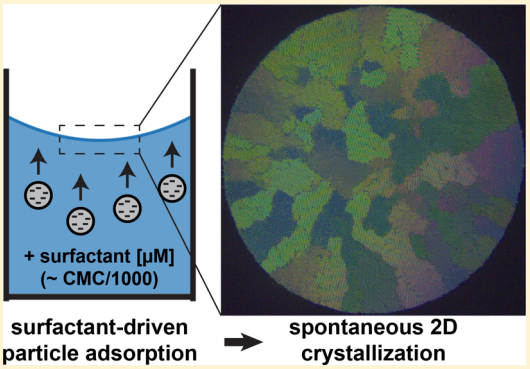

INTRODUCTION

Controlling adsorption and two-dimensional (2D) organization of particles at a fluid interface is a crucial process[1] that is directly involved in numerous industrial, environmental, and technological applications.[2,3] From a fundamental viewpoint, particles at interfaces also provide both a rich playground for studying physical phenomena in two dimensions[4−13] and an invaluable technological platform for the development of functional materials with tunable properties.[14−17] In this study, we describe a new and remarkably simple way to induce the adsorption of colloidal particles at an air−water interface and further control their 2D organization. We show that, when a minute amount of a cationic surfactant is added to a dilute aqueous suspension of anionic microparticles, a significant number of particles adsorb at the air−water interface. Depending on both surfactant and particle concentrations, we find that the adsorbed particles can organize into various 2D structures, from closely packed colloidal crystals to loosely packed gels.

Our strategy markedly differs from what has been reported so far regarding the 2D self-assembly of colloidal particles at a fluid interface in the following aspects. First, in our approach, the particles are transported from the bulk of the suspension to the air−water interface where they directly adsorb. This is in contrast to most studies, where a small amount of an external suspension of particles in an organic solvent is spread on the surface of an aqueous solution (usually exempt of particles). This forces the particles to stay at the air−water interface after the evaporation of the organic solvent.[3] This spreading

Received: September 24, 2018
Revised: October 23, 2018
Published: November 11, 2018

DOI: 10.1021/acs.langmuir.8b03233
Langmuir 2018, 34, 15526−15536

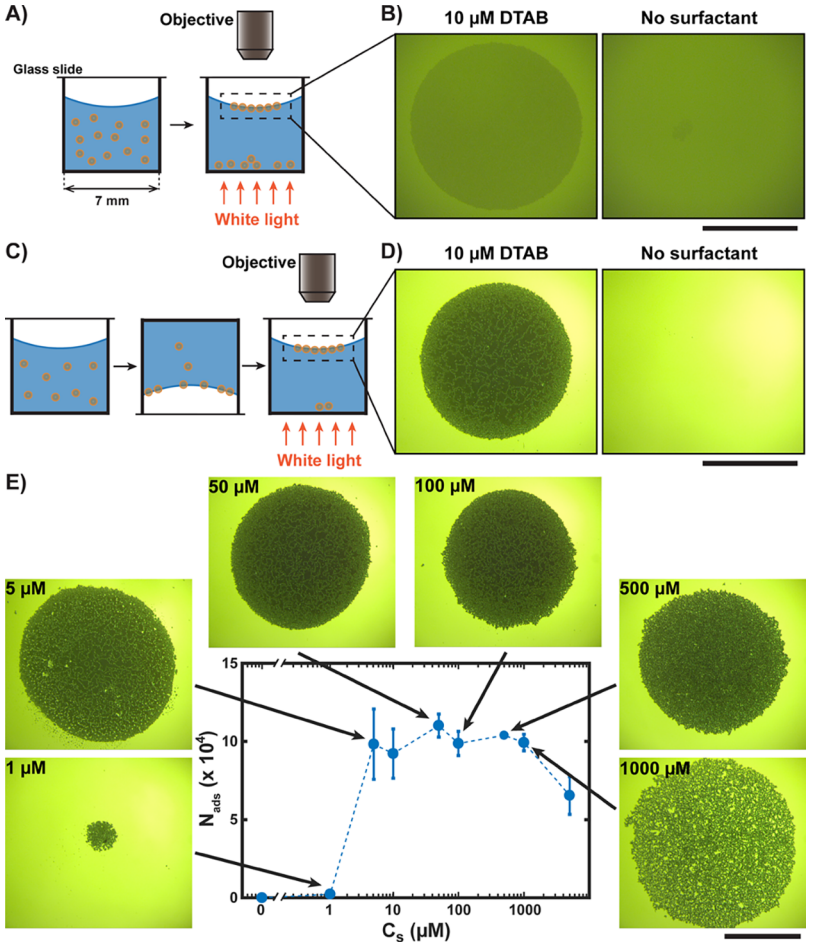

Figure 1. Cationic surfactant (DTAB) induces the adsorption of negatively charged PS microparticles (diameter = 5.1 μm) at the LG interface leading, at concave interfaces, to circular 2D colloidal assemblies. (A) "Straight method": the surfactant/particle mixture is placed in a cylindrical (diameter 7 mm) cell covered with a glass slide to avoid evaporation and is left unmoved overnight. A 2D patch of particles spontaneously forms at the center of the concave LG interface, whereas nonadsorbed particles sediment at the bottom of the cell. (B) Brightfield transmission microscopy image of the LG interface with a particle concentration of C_p = 5 mg/mL, in the presence (left) and absence (right) of DTAB, C_s = 10 μM. (C) "Flipping method": the surfactant/particle mixture is placed in the cell prior to flipping it upside down so that gravity brings the particles to the LG interface. After 2 h, the sample cell is flipped back to its original position. Adsorbed particles accumulate at the center of the concave interface to form a 2D colloidal patch. (D) Brightfield transmission microscopy image of the LG interface with a particle concentration of C_p = 0.05 mg/mL, in the presence (left) and absence (right) of DTAB, C_s = 10 μM. (E) Number of particles adsorbed at the LG interface, N_{ads}, as a function of DTAB concentration using the flipping method. Brightfield transmission microscopy images show the corresponding 2D colloidal assemblies: disordered (C_s = 1 μM), densely packed and polycrystalline (C_s = 5−100 μM), densely packed and disordered (C_s = 500 μM), and loosely packed gels (C_s = 1 mM). Symbols and error bars show mean values ± standard deviation (SD) from three individual experiments. All scale bars are 1 mm.

methodology has been widely used to study the behavior of particle monolayers at the air−water interface, especially during compression or expansion in Langmuir troughs.[18] Second, we report an effect of the surfactant at concentrations 100−1000 times lower than what has been investigated so far. Indeed, oppositely charged surfactants have been extensively exploited to alter the surface properties of particles and therefore to mediate their interaction with a fluid interface.[19] More specifically, surfactants at high enough concentrations are known to electrostatically adsorb on oppositely charged hydrophilic particles, thus altering their wettability. At the surfactant concentration regime where particles become hydrophobic enough, the latter could adsorb at the air−water interface.[20] This very efficient approach has been exploited to stabilize foams[21] and emulsions,[22] or for other applications such as the suppression of the coffee-ring effect.[23,24] However, achieving such a level of hydrophobization typically requires a sufficiently large amount of the adsorbed surfactant typically leading to particle neutralization. Compared to the critical micellar concentration (CMC), such effects are usually achieved with a concentration of the order of CMC/10 for ionic surfactants adsorbing on hydrophilic surfaces.[25−27] As a result, the neutralized particles become barely repulsive and thus poorly prone to crystallization. Velikov et al. could produce colloidal crystals in that surfactant concentration regime in the particular geometry of microparticles confined in thinning foam films.[28] The conjunction of surfactant-induced particle hydrophobization and application of mechanical force led to particle adsorption at both the top and bottom interfaces, as well as long-range hexagonal ordering of the interfacial particles upon stepwise compression of the films.

Here, for the first time, we demonstrate that, without applying any additional external force, a strikingly smaller amount of cationic surfactant is enough to induce the adsorption of negatively charged particles to a static air−water interface without modifying the particle surface properties. At these

DOI: 10.1021/acs.langmuir.8b03233
Langmuir 2018, 34, 15526−15536

concentrations, which are typically 3−4 orders of magnitude lower than the CMC, surface tension effects are negligible. Furthermore, by means of zeta potential measurements, we demonstrate that there is no significant surfactant adsorption on the particle surface. As a result, the adsorbed particles at the interface maintained most of their initial charge, being able to organize and eventually crystallize there. We suggest that it is the preferential adsorption of the surfactant at the air−water interface that diminishes the electrostatic barrier for particle adsorption on the like-charged interface and therefore facilitates the adsorption of anionic particles there.[29] To our knowledge, such an "electrostatic shielding" effect, which is reminiscent of the role of salts in mediating particle adsorption at the air−water interface,[29−31] has never been described using surfactants. A striking advantage of surfactants over simple salts is their inherent ability to accumulate at the interface, and therefore to increase their local shielding efficiency. As a result, we show that particle adsorption and crystallization can be induced at micromolar concentrations of the surfactant, which are at least 3 orders of magnitude smaller than typical electrolyte concentrations used to promote particle adsorption.

We exploit this new principle and describe two practical ways to induce the adsorption of anionic particles at the air−water interface without neutralizing them. Through a combination of wide-field transmission and confocal reflection microscopies, we analyze the adsorbed particle monolayers and explain how both surfactant and particle concentrations control the way particles organize at the interface. We establish a phase diagram evidencing a wide range of conditions where extended 2D colloidal crystals can be obtained in a reproducible way. Finally, we demonstrate that this same principle can be applied to crystallize two different types of microparticles (anionic polystyrene (PS) and silica) as well as nanoparticles, suggesting that the approach is operational irrespective of specific physicochemical particle properties. Overall, our findings provide both a new look at particle behavior at fluid interfaces and a useful guideline for the controlled preparation of 2D materials in a novel, robust, and versatile manner.

RESULTS AND DISCUSSION

Particle Adsorption and 2D Organization at the Air−Water Interface. Figure 1 shows a schematic representation of our experiments. We mixed a dilute aqueous suspension of anionic PS microparticles (cross-linked particles with both sulfate and high density of carboxyl functional groups on their surface, diameter 5.1 μm) with an aqueous solution of cationic surfactant dodecyltrimethylammonium bromide (DTAB) in an Eppendorf tube. The concentration of microparticles and the surfactant in the final mixture was C_p = 5 mg/mL and C_s = 10 μM, respectively (CMC = 13.4 mM at 25 °C[24]). We transferred 200 μL of the mixture to a cylindrical (diameter 7 mm) chamber, and we placed a glass coverslip on it to prevent water evaporation. The aqueous mixture partially wetted the walls of the chamber (contact angle ≈ 80°), resulting in a slightly concave air−water interface. The sample was placed on the stage of a home-built upright microscope and was left unmoved overnight at room temperature (22 ± 2 °C). We called this process, which did not involve any manipulation of the sample cell, the "straight method" (Figure 1A). Inspection of the sample with brightfield transmission microscopy revealed that, whereas most of the microparticles accumulated at the bottom of the chamber due to sedimentation, a significant number of particles were spontaneously adsorbed at the liquid−gas (LG) interface. These interfacial particles formed a 2D colloidal crystal at the center of the LG interface, that is at the middle of the chamber (Figure 1B, left). A representative movie, recorded shortly after loading the surfactant/particle mixture in the chamber, showing the formation of the 2D crystal is provided in the Supporting Information (Movie S1). We hypothesized that DTAB was responsible for promoting the adsorption of particles to the LG interface and their subsequent crystallization in two dimensions. To test this hypothesis, we repeated the same experiment in pure water (no surfactant), and we found that almost no particles were adsorbed at the air−water interface (Figure 1B, right). We attributed the transport of the particles to the free interface to convection. Flow visualization experiments revealed that convective flows were always present in our samples, presumably due to unavoidable small variations in ambient temperature (of the order of 0.1 °C). Hence, we devised another simple method to realize a controlled transport mechanism that would bring particles to the LG interface in a fully controllable fashion. We called it the "flipping method" (Figure 1C). After loading the chamber with the surfactant/particle mixture, we inverted the chamber and left it in this position for 2 h. Note that the capillary forces prevented the liquid from flowing out of the chamber. We maintained the surfactant concentration the same as for the straight method (C_s = 10 μM); however, we employed a much lower particle concentration, C_p = 0.05 mg/mL. We chose this C_p because (i) it should yield a surface coverage similar to that in the straight method (assuming that all particles adsorb to the free interface) and (ii) the absence of sedimented particles at the bottom of the chamber would allow for better transmission imaging because of the absence of strong scattering. After 2 h, we inverted the chamber once again to bring it to its initial position (Figure 1C). Similar to the straight method, we observed the formation of a circular 2D polycrystalline patch (Figure 1D, left), having a diameter of 1.8 ± 0.1 mm composed of monocrystalline domains (dark zones inside the patch) separated by boundaries (bright lines inside the patch). We analyzed the crystallization process of particles adsorbed at the LG interface by recording their behavior soon after the second flipping process (Movie S2). We observed that, similar to the "straight method", particles first accumulated at the center of the chamber where the interface curvature was maximum, prior to progressively crystallizing from the center of the patch to its edge. The whole process (particle assembly and crystallization) took about 5 h. A control experiment using the same colloidal suspension but without the surfactant yielded no particle adsorption at the LG interface, and thus no 2D structure was formed (Figure 1D, right). We conducted further experiments by mixing the particle suspensions with anionic (sodium dodecyl sulfate, Figure S1) or nonionic surfactant (triethoxy monooctylether, Figure S2), and we found that almost no particles were adsorbed at the interface. All these findings indicate that a micromolar amount of the DTAB cationic surfactant induced the adsorption of anionic particles at the air−water interface. Once adsorbed, these particles accumulated at the center of the concave interface where they self-organized into a mm-sized, 2D polycrystalline colloidal crystal.

Influence of Surfactant Concentration on Particle Adsorption and Interparticle Interactions at the Air−Water Interface. To elucidate the role of the surfactant in adsorption and further crystallization of the suspended particles at the LG interface, we used the "flipping method" at a fixed particle concentration (C_p = 0.05 mg/mL) and varying DTAB concentration. We measured the number of particles adsorbed

DOI: 10.1021/acs.langmuir.8b03233
Langmuir 2018, 34, 15526−15536

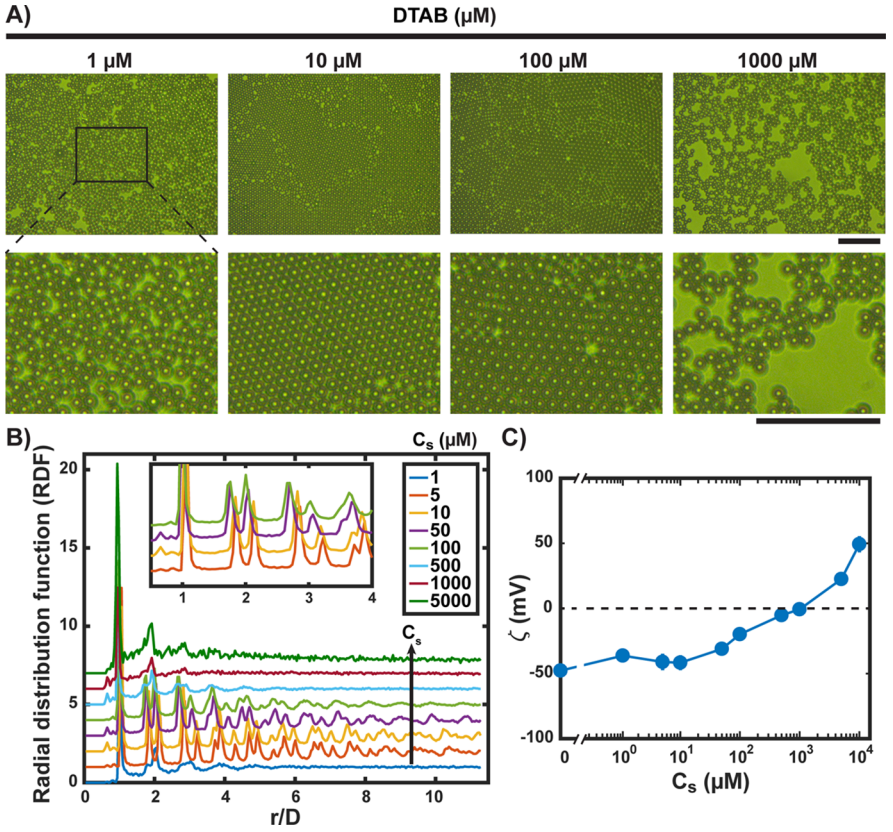

Figure 2. DTAB concentration tunes the organization of anionic PS particles (diameter = 5.1 μm) adsorbed at the LG interface using the "flipping method". (A) Representative brightfield transmission microscopy images of the 2D colloidal assemblies as a function of DTAB concentration (given), at a fixed particle concentration C_p = 0.05 mg/mL. Zoomed images of the central area of the assemblies (indicated by a black rectangle) are shown in the bottom row. The scale bars are 50 μm. (B) RDF computed from images as in (A) top row, as a function of DTAB concentration (C_s); r is the interparticle distance and D is the particle diameter. The RDFs are vertically offset for the ease of comparison. The inset shows a magnified view of the first peaks, revealing a shift toward shorter interparticle distances upon increasing surfactant concentration. (C) Zeta potential (ζ) measurements of mixtures of PS particles (C_p = 0.05 mg/mL) with varying concentrations of DTAB. Symbols represent mean values of six independent measurements. The error bars (SD, not shown) are smaller than the symbol size.

at the LG interface (N_{ads}) as a function of C_s (Figure 1E). As mentioned earlier, there was no particle adsorption for the surfactant-free dispersions. For C_s = 1 μM, only a small amount ($N_{ads} \approx 2.3 \times 10^3$) of particles was adsorbed to the free interface. These particles formed a small disordered patch of roughly circular shape. Raising the DTAB concentration to C_s = 5 μM led to a dramatic increase in the number of adsorbed particles, with N_{ads} reaching a value of about 10^5 and the formation of a dense circular patch with a diameter of 1.8 ± 0.2 mm. Further increasing the DTAB concentration, in the range C_s = 10−500 μM, did not result in an increase of N_{ads}, which remained of the order of ~10^5 particles. Strikingly, this N_{ads} was very close to the total number of particles in suspension (1.4×10^5), confirming that using the "flipping method" at this particle concentration, the majority of suspended particles adsorbed at the LG interface. Although particles always formed circular patches of approximately a constant diameter, the microstructure of the colloidal assemblies was dependent on C_s. For C_s = 5−100 μM, all patches displayed a polycrystalline structure except at their edges where particles were less ordered. For C_s = 500 μM, particles were organized in a dense but amorphous circular patch. For C_s = 1 mM, whereas N_{ads} remained unaltered ($N_{ads} \approx 10^5$), the adsorbed particles formed a loosely packed circular patch of an increased diameter of ~2.2 mm. Notably, the number of adsorbed particles decreased with further increasing the DTAB concentration, reaching $N_{ads} = 6.5 \times 10^4$ for C_s = 5 mM.

To investigate the evolution of the microstructure of the 2D colloidal assemblies as a function of surfactant concentration, we examined the central part of the patches by means of high magnification transmission microscopy (Figures 2A and S3). We quantified the observed structural evolution by computing the radial distribution function (RDF) from these images (Figure 2B). For C_s = 1 μM, the particles were organized in a relatively dense arrangement but with no long-range order (Figure 2B, blue curve). In striking contrast, for C_s = 5−10 μM, particles were arranged in a closely packed hexagonal lattice with only a few defects (Figure 2B, red and yellow curves). The corresponding RDF confirmed the long-range positional order, showing clear peaks up to distances (r) normalized with respect to the particle diameter (D) of r/D = 10. This increased positional order was maintained for r/D = 6 for higher DTAB concentrations, up to C_s = 100 μM. For C_s = 500 μM, most of the long-range order was lost, whereas for $C_s \geq 1$ mM, the structure was disordered with patches adopting a 2D gel-like morphology (Movie S3). Moreover, in the region where crystallization occurred (C_s = 5−100 μM), the RDF analysis showed that the positions of the first peaks were shifted to lower r/D values upon increasing C_s, indicating repulsive particles assembling at a closer distance to each other with an increase in C_s (inset of Figure 2B). In particular, the position of the first peak decreased progressively from $r_1/D \approx 1.1$ to nearly 1.0, showing that particles were very close but not in contact when they

DOI: 10.1021/acs.langmuir.8b03233
Langmuir 2018, 34, 15526−15536

crystallized. The role of surfactant concentration was thus shown to be instrumental in controlling both the adsorption and organization of particles at the LG interface. Adding a small amount of surfactant promoted particle adsorption but adding too much resulted in amorphous gel-like structures of "sticky" particles. Crystallization thus occurred at a specific C_s range where particles repelled each other with an interparticle distance that decreased with an increase in C_s.

Role of the Electrostatic Surface Properties of the Particles. To investigate how the electrostatic properties of particles were affected by the presence of DTAB, we measured the zeta potential (ζ) of the aqueous particle suspensions under the conditions used in Figure 2A,B, by maintaining C_p = 0.05 mg/mL and varying C_s (Figure 2C). Note that these measurements were performed in the bulk, and the exact surface potential of particles adsorbed at the air−water interface might differ from these values. However, as we will show later, about 94% of the adsorbed particle diameter remains in the bulk phase. Therefore, although local rearrangement of surfactants on the particle surface can occur at the vicinity of the interface upon particle adsorption, we can assume that the values measured in the bulk can be used as good semiquantitative estimation of how particles electrostatically interact once adsorbed at the interface. The PS particles displayed a negative surface potential of ζ = −50 mV in pure water, as a result of their dissociable surface groups (being mostly carboxylic acid). For DTAB concentrations up to C_s = 10 μM, ζ retained this value, indicating that in this C_s range, there was no significant surfactant adsorption on the surface of the particles. With increasing DTAB concentration, the magnitude of the zeta potential started to decrease, assuming values of ζ = −31 mV and ζ = −20 mV for C_s = 50 μM and C_s = 100 μM, respectively. Further addition of DTAB led to the neutralization (C_s = 0.5−1 mM) and then to the sign reversal (C_s = 5−10 mM) of the zeta potential, attributed to the formation of a monolayer and then a bilayer of DTAB molecules on particle surfaces, respectively.[24] Particles adsorbed at the LG interface thus significantly crystallized, that is, displayed a long-range order, only when they remained highly negatively charged and thus repulsive ($5 \leq C_s \leq 100$ μM). In this C_s range, the correlation between the slight decrease in $|\zeta|$ and the decrease in the interparticle distance (Figure 2B, inset) shows that the surfactant concentration tuned the interparticle distance in crystal domains through the modulation of the electrostatic repulsion potential between the particles. Similarly, amorphous and gel-like structures were obtained when the surfactant neutralized the particles (C_s = 0.5−1 mM). All these results show that short-range interparticle repulsion was necessary for crystallization to occur, which occurred at a surfactant concentration significantly lower than that necessary to neutralize particles.

Effect of Particle Concentration on 2D Crystallization. We observed that, at a very low surfactant concentration, particles did adsorb while keeping a highly negative surface, but they did not crystallize. For instance, although crystals were formed at C_s = 10 μM, no crystallization occurred at C_s = 1 μM and C_p = 0.05 mg/mL (Figure 2A) despite a highly negative zeta potential (ζ = −36 mV). Interestingly, this situation corresponded to a marked different amount of adsorbed particles: $N_{ads} = 2.3 \times 10^3$ and 8.0×10^4 for C_s = 1 and 10 μM, respectively (Figure 1E). We explain this difference by a higher amount of surfactant at the air−water interface, and therefore a stronger electrostatic shielding, when increasing C_s. To assess whether crystallization could occur at ultralow surfactant concentration but for a higher number of adsorbed particles, we used the "flipping method" to prepare colloidal patches for various particle concentrations at a fixed C_s = 1 μM. For very dilute suspensions (C_p = 0.01 mg/mL), almost no particles were present at the LG interface (N_{ads} = 290). A gradual increase in N_{ads} was observed with increasing particle concentration from C_p = 0.05 mg/mL to C_p = 1 mg/mL, with the respective values being $N_{ads} = 2.3 \times 10^3$ and $N_{ads} = 8 \times 10^3$. Further raising C_p to 5 mg/mL resulted in a more drastic increase in N_{ads}, which assumed a value of 2.3×10^4 (Figure 3A).

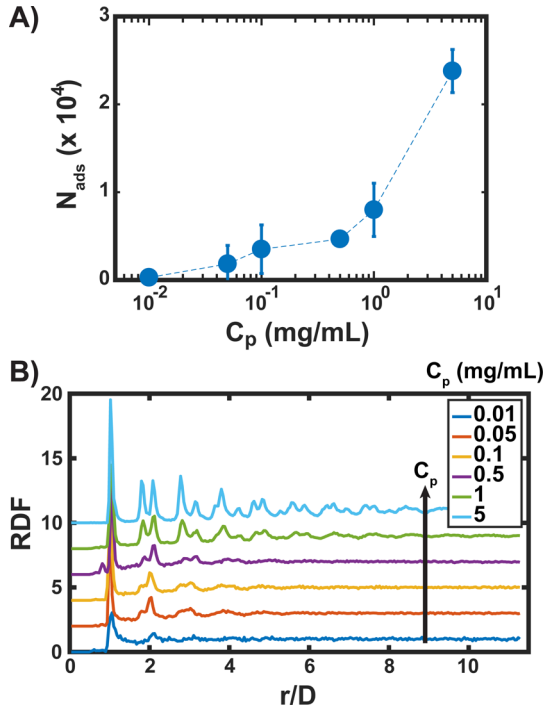

Figure 3. Raising the particle concentration C_p increases the number of particles adsorbed at the LG interface and promotes 2D colloidal crystallization in patches prepared at a fixed DTAB concentration (C_s = 1 μM) using the "flipping method" with anionic PS particles (diameter = 5.1 μm). (A) Number of adsorbed particles (N_{ads}) at the LG interface as a function of particle concentration. Symbols and error bars show mean values ± SD from three individual experiments. (B) RDF computed from the images of the colloidal assemblies for different values of C_p; r is the interparticle distance and D is the particle diameter. The RDFs are vertically offset for clarity.

The number of interfacial particles had a profound effect on the microstructure of the 2D colloidal assemblies, as demonstrated by the corresponding RDF shown in Figure 3B (microscopy images are shown in Figure S4). For the lowest particle concentration (C_p = 0.01 mg/mL) and hence the minimum number of adsorbed particles, the resulting structure was relatively closely packed but lacked any long-range order. For C_p = 0.05−0.5 mg/mL, the degree of order increased as shown by the emergence of sharp peaks at r/D = 2 and r/D = 3 in the RDF. Interestingly, further increasing the number of adsorbed particles by using more concentrated suspensions drastically improved the degree of the 2D order, which extended to distances r/D = 7 and r/D = 9 for, respectively, C_p = 1 mg/mL and C_p = 5 mg/mL, corresponding to $N_{ads} = 8 \times 10^3$ and $N_{ads} = 2.3 \times 10^4$, respectively. Note that a similar evolution from disordered to more ordered structures with increasing C_p was also observed at a higher C_s (10 μM, Figure S5) but required

DOI: 10.1021/acs.langmuir.8b03233
Langmuir 2018, 34, 15526−15536

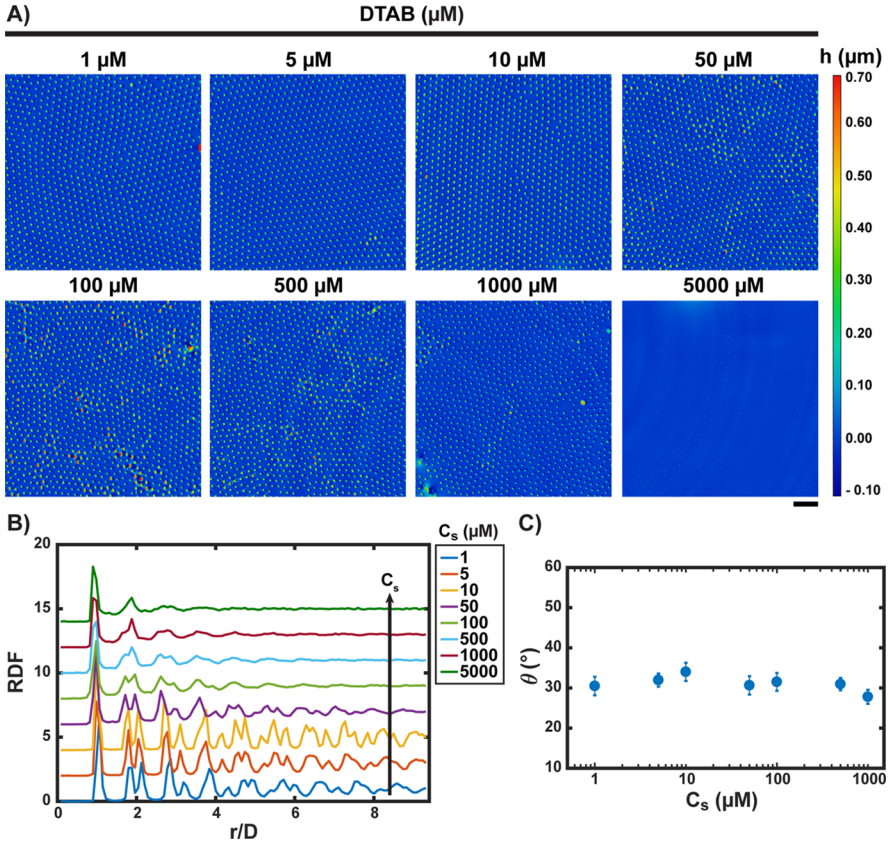

Figure 4. In situ confocal microscopy experiments reveal the exact positioning in three dimensions of the PS microparticles at the LG interface obtained using the "straight" method. (A) Height images of the interfacial particle assemblies obtained by varying C_s (given) at C_p = 5 mg/mL. h is the height protruding into air. The scale bar is 20 μm. (B) RDF corresponding to the height images shown in (A). RDFs are vertically offset for ease of comparison. (C) Average value of the contact angle that each PS particle forms with the LG interface as a function of C_s. There is no point at 5 mM as the images were not analyzable because of the very small h values. Details of these measurements are included in Figure S7.

lower values of C_p. All these results show that a sufficiently high number of adsorbed particles are necessary for crystallization to occur and that the range of the crystalline order increases with increasing N_{ads}, a parameter that is directly controlled by C_p. We attribute this effect to the so-called "collective sinking effect",[32] which accounts for the collective deformation of the interface due to the presence of a large number of adsorbed particles. Increasing C_p and therefore N_{ads} enhances the collective deformation of the interface, which in turn induces a long-range gravity-driven attraction potential toward the interface center, leading in the end to long-range crystallization.

Comparison between the "Straight" and "Flipping" Method Experiments. As mentioned earlier (Figure 1), the adsorption and the self-organization behavior of the particles at the LG interface were qualitatively similar for the "straight" and "flipping" methods. It is interesting at this point to scrutinize in more detail the microstructural properties of the interfacial colloidal assemblies resulting from these two methods. We begin by discussing the assemblies formed with the "straight" method using a fixed particle concentration (C_p = 5 mg/mL) and varying C_s. We utilized white light-based reflection confocal microscopy to visualize the structure of the assemblies with higher vertical and lateral resolution, as well as to quantitatively map the vertical positioning of single particles at the LG interface, as discussed later in more detail. The height images corresponding to particle monolayers formed at different surfactant concentrations are shown in Figure 4A, and the respective RDFs are presented in Figure 4B. Highly organized polycrystalline patches were formed for all DTAB concentrations in the range C_s = 1−100 μM. However, the long-range order of the interfacial structures was dependent on the value of C_s. Well-ordered crystals for distances up to r/D = 9 were observed for C_s = 1−50 μM, with the interparticle distance decreasing with increasing C_s. The range of the order considerably decreased for C_s = 100−500 μM while largely disordered particle monolayers were observed for $C_s \geq 1$ mM. These results are in accordance with the ones obtained with the "flipping" method at the much lower particle concentration C_p = 0.05 mg/mL, except for the extreme cases of very low and very high C_s. With the "straight" method, well-ordered crystals were obtained for C_s = 1 μM, whereas the "flipping" method led to the formation of an amorphous closely packed colloidal patch. This dissimilarity can be explained by the difference in the number of adsorbed particles, which was larger with the straight method because of the much higher C_p (Figure S6). This is also in agreement with the fact that crystals were obtained at C_s = 1 μM using the "flipping" method by increasing C_p (Figure 3). For C_s = 5 mM, the number of adsorbed particles obtained with the "straight" method was very low (Figure 4A), whereas it remained significant with the "flipping" method (Figure 1E). We attribute this difference to the formation of particle aggregates at such C_s and the different mechanisms that transport particles to the interface. With the "flipping" method, gravity was able to bring both single particles and aggregates to the LG interface, resulting in a high number of adsorbed particles. In contrast, with the "straight" method, convection

DOI: 10.1021/acs.langmuir.8b03233
Langmuir 2018, 34, 15526−15536

more selectively transported single particles, and therefore, only a small number of particles could reach the LG interface.

The results from both the "straight" and "flipping" methods show that DTAB concentration of the order of μM induced the adsorption of particles at the LG interface, regardless of the mechanism of transport (convection and sedimentation, respectively). Adsorbed particles crystallized only when they remained charged and, in that regime, surfactant concentration tuned the interparticle distance in the colloidal crystal. For the "flipping" method, where the mechanism responsible for transporting particles to the interface was well controlled, increasing the particle concentration in the suspension led to a larger number of interfacial particles, which in turn favored particle ordering.

Elucidating the Role of the Particle Contact Angle at the LG Interface. From the confocal images of the particles at the LG interface (Figure 4A), we measured the maximum height (h) protruding in air for each particle. This allowed us to calculate the contact angle (θ) measured through water that each individual particle made with the air−water interface, $\theta = \arccos((D - 2h)/D)$ (Figure S7). Confocal microscopy was used in the past and shown to extract reliable values of the contact angle of single particles.[33] Here, we expanded this principle to measure in situ the contact angle of a large number of individual microparticles at the LG interface. Figure 4C shows the evolution of θ, averaged from about 10^3 individual particles, as a function of C_s for C_p = 5 mg/mL. Interestingly, the contact angle that the particles made with the LG interface did not depend on DTAB concentration for C_s = 1 μM to 1 mM, assuming a value of $\theta \approx 30°$. This constant value of θ shows that changes in the wettability of the particles were not at the origin of the marked evolution of particle organization at the LG interface, from highly crystalline to amorphous structures when C_s increased from 1 μM to 1 mM. Moreover, the value of $\theta \approx 30°$ corresponds to a protruding fraction of the particle diameter into air of only $P = h/d \approx 6\%$. This strong immersion of particles in the water phase shows that the short-range electrostatic repulsion between adsorbed particles was mostly affected by the surface charge of particles in water. The zeta potential evolution measured in bulk (Figure 2C) was thus a good estimation of how this surface charge was affected by the concentration of the surfactant and how in turn it directly controlled the organization of adsorbed particles.

Proposed Explanation for Particle Adsorption at a Very Low Cationic Surfactant Concentration. First, we have discovered that an amount of the DTAB cationic surfactant of the order of C_s = 1−10 μM (i.e., 3 to 4 orders of magnitude lower than the CMC = 13.4 mM) induced the adsorption of anionic PS microparticles at the LG interface. It is known that ionic surfactants adsorb onto oppositely charged particles and can in turn induce their adsorption to fluid interfaces, by significantly decreasing their charge and/or increasing their hydrophobicity.[20,34] This is, however, not the mechanism explaining particle adsorption at such a low C_s observed in our experiments. As we demonstrated by zeta potential measurements in bulk (Figure 2C) and in situ measurements of the particle contact angles at the LG interface (Figure 4C), particles adsorbed at C_s where their wetting and electrostatic properties were almost unaffected by the presence of the surfactant. We suggest instead that the main role of the surfactant was through their adsorption at the air−water interface. We propose that the amount of the adsorbed cationic surfactant at the LG interface, although very small, was enough to reduce the energy barrier between adsorbing anionic particles and the like-charged LG interface, which is the result of both the repulsive van der Waals and electrostatic interactions between them.[29,35] An effect qualitatively similar to the surfactant-driven effect described here has been reported in similar PS latex suspensions, where the addition of simple electrolytes resulted in enhanced particle adsorption to the air−water interface.[29,31] In addition, organic salts with hydrophobic ions have been used for promoting the adsorption of oppositely charged nanoparticles to oil−water interfaces.[36] The height of the adsorption barrier, described by the classical Derjaguin−Landau−Verwey−Overbeek theory after considering the effects of the solvation zone around the particles and the air−water interfacial regions, decreased with increasing ionic strength of the suspension.[31] We believe that the surfactant cations have an action similar to electrolytes; however, they are more effective than the latter as they can work at very low concentrations because of their preferential accumulation at the LG interface, acting effectively as "super-salts". Our suggested mechanism is confirmed by our observation that using anionic surfactant instead of the cationic surfactant did not induce particle adsorption (Figure S1) presumably because they increase the electrostatic adsorption barrier for anionic particles.

Proposed Mechanism and Phase Diagram of Interfacial Particle Organization. Based on our results, we can propose a general mechanism for the adsorption and subsequent organization of anionic particles at the air−water interface, in the presence of a small amount of cationic surfactant. Cationic surfactant-induced particle adsorption at concentration C_s was large enough to decrease the electrostatic barrier for particle adsorption at the interface but small enough for the particle charge to be preserved (Figure 2C), thus resulting in short-range electrostatic repulsion between adsorbed particles which were mostly immersed in the water phase (Figure 4C). Once adsorbed, the interfacial microparticles did not leave the free interface, which was due to the reduction of the total surface energy associated with the transport of the particles from the bulk to the partially wetted state at the interface,[37] resulting in the capillary trapping of particles at the interface in agreement with earlier work. The contact angle of the particle/surfactant aqueous mixture with the walls of the sample cell was always less than 90°, resulting in a concave meniscus (Figure S8). As a result, all adsorbed particles were subjected to a curvature-driven gravity transport toward the center of the LG interface, resulting in a long-range attractive potential toward the center of the patch. The combination of this long-range attraction with the short-range electrostatic repulsion at low C_s led to particle organization into polycrystalline patches. We can thus discuss how both surfactant (C_s) and particle (C_p) concentrations controlled the way particles organized once adsorbed at the LG interface. The general trend was that increasing C_s, by promoting surfactant adsorption both at the LG interface and onto the surfaces of the particles, decreased the electrostatic potential between particles. This first resulted in a decrease in the interparticle distance within the colloidal crystals accompanied by a progressive loss of the long-range order. At large C_s, particles were not repulsive anymore and formed amorphous gels. Increasing C_p, by increasing the number of adsorbed particles, led to a stronger long-range attraction potential because of the collective deformation of the interface by adsorbed particles. It thus promoted crystallization for surfactant concentrations at which adsorbed particles remained repulsive. To analyze the synergistic role of these two

DOI: 10.1021/acs.langmuir.8b03233
Langmuir 2018, 34, 15526−15536

parameters, we built a phase diagram where we represented the experimentally observed state, that is amorphous or crystal, as a function of C_s and C_p (Figure 5). In this phase diagram, four

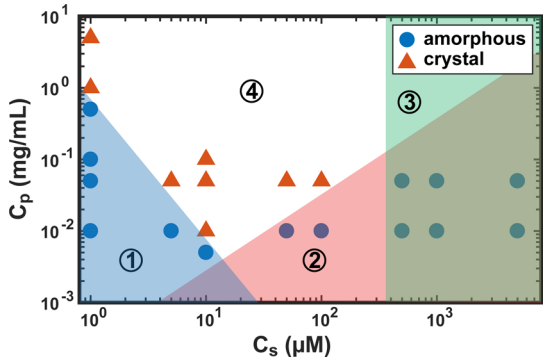

Figure 5. Phase diagram of the patch organization as a function of PS particle and DTAB surfactant concentrations. Symbols are experimental data depicting an amorphous (sphere) or a polycrystalline (triangle) state. The background colors qualitatively depict four zones (see main text for details).

zones were qualitatively distinguished. At low C_s and C_p, the number of adsorbed particles was very small, resulting in a too weak long-range attractive potential: the particles thus formed a disordered phase (zone 1). At a given C_s, increasing C_p promoted particle crystallization by the "collective sinking mechanism", an effect becoming weaker when the number of adsorbed particles induced by the surfactant increased, that is, by increasing C_s. The slope between zones 1 and 4 was thus negative. At a moderately higher C_s but low C_p (zone 2), particles did not crystallize because they were partially neutralized by the surfactant. Increasing C_p at constant C_s again promoted crystallization, but this effect became stronger with a decrease in particle charge, that is, when C_s increased. The slope between zones 2 and 4 was thus positive in that case. With a further increase in C_s, particles became almost fully neutralized by the surfactant, leading to sticky particles within the patches. The adsorbed particles thus formed amorphous gels, most probably regardless of particle concentration (zone 3). Zone 4 thus corresponds to the situation where both C_s and C_p allowed the adsorption and organization of a large number of repulsive particles into 2D polycrystalline patches.

Generalization of the 2D Crystallization Method with Other Surfactants and Particles. We hypothesized that our 2D crystallization method should be applicable to different anionic particle/cationic surfactant systems. To assess its breadth of applicability, we first kept the same PS anionic particles but replaced DTAB with a more hydrophobic cationic surfactant, hexadecyltrimethylammonium bromide (CTAB). As expected, CTAB induced particle adsorption and crystallization at the LG interface in a way similar to DTAB (Figures S9–S11). Particle adsorption was, however, promoted at a lower C_s (Figure S9 cf. Figure 1), which we attribute to the higher surface activity of CTAB (CMC = 0.92 mM[24]), implying that a lower amount of the surfactant was enough to efficiently decrease the adsorption barrier. Interestingly, the formation of gels was also observed at C_s corresponding to particle neutralization (Figures S9 and S10) and the contact angle adopted approximately the same constant value ($\theta \approx 30°$) as with DTAB (Figure S11).

Next, we kept DTAB as the cationic surfactant but used hydrophilic anionic silica particles (diameter 4.6 μm, possess surface silanol groups) instead of anionic PS particles. Because silica particles (1.85 g/cm^3 according to the manufacturer) are denser than PS particles (1.06 g/cm^3), we used the "flipping" method to study their adsorption and crystallization behavior at the LG interface. In the case of surfactant-free dispersions, we observed no particle adsorption at the air–water interface (Figure S12). On the contrary, 2D crystals were obtained when

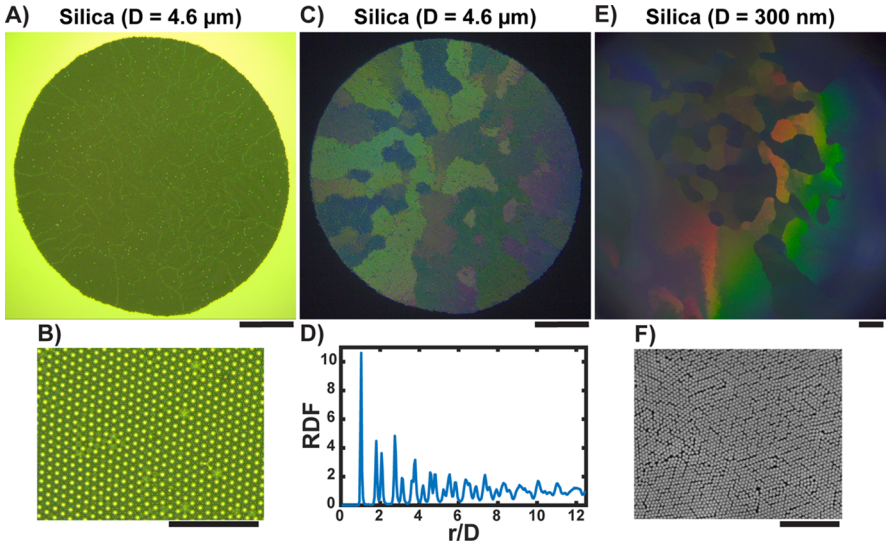

Figure 6. DTAB induces the adsorption and subsequent crystallization of both micrometer- and nanometer-sized negatively charged silica particles at the LG interface. (A) Transmission microscopy image of a 2D polycrystalline patch of 4.6 μm diameter particles obtained with the "flipping" method at C_s = 10 μM and C_p = 0.05 mg/mL. (B) High magnification image of the central region of the colloidal patch in (A). (C) Reflection image of the same sample as in (A) obtained using white light illumination from the side of the chamber. The emergence of structural colors allows one to distinguish adjacent monocrystalline domains. (D) RDF computed from an area of 250 μm × 190 μm of the colloidal crystal in (A). (E) Reflection image obtained in the same conditions as in (C) but with 300 nm particles (C_s = 5 μM; C_p = 0.05 mg/mL). (F) SEM image of the colloidal patch after deposition on a glass substrate. The scale bars are 300 (A,C,E), 50 (B), and 5 μm (F).

DOI: 10.1021/acs.langmuir.8b03233
Langmuir 2018, 34, 15526–15536

DTAB was added to the suspension at the same concentration (C_s = 10 μM) as in the case of PS particles (Figure 6A–D). Interestingly, the entire colloidal assembly was crystalline in the case of silica particles, a feature never observed in the case of PS particles. Additionally, because of their higher density, the silica particles quickly accumulated at the center of the LG interface, resulting in a much faster crystallization kinetics compared to the case of the PS particles of similar size (Movie S4). Under our experimental conditions, crystallization occurred simultaneously with particles gathering at the center of the LG interface, resulting in the whole patch being formed and fully crystallized in typically 20 min after the second flipping of the cell. We believe that those aspects are a direct consequence of the "collective sinking effect",[32] which was more pronounced in the case of silica microparticles because of their higher density. Finally, we observed that the monocrystalline domains were generally composed of a higher number of particles compared to the PS case, presumably due to the lower size polydispersity of the silica particles. Interestingly, the highly ordered organization of silica particles led to structural optical properties. With a lateral white light illumination, the patches displayed selective reflection, allowing one to distinguish adjacent monocrystalline domains through the color shift induced by the abrupt change in domain orientation (Figure 6C).

We applied the same protocol with submicrometer-sized silica particles (300 nm in diameter) but using a longer time (~20 h) for particle sedimentation after the first flipping step. Notably, we could observe the appearance of a similar structural colored pattern indicating the formation of an ordered layer composed of adjacent, monocrystalline, and mm-sized domains of nanoparticles (Figure 6E). To further scrutinize the particle organization, we deposited this layer on a glass substrate by slow evaporation of the water solution. Scanning electron microscopy (SEM) analysis of the deposited assembly revealed a long-ranged hexagonal packing of particles in close contact (Figure 6F). Note that, with this method of deposition, because of interface curvature, the evaporation led to the contact of the particle layer with the substrate starting from its center followed by a strong lateral stress when the surrounding liquid continued to evaporate. This mechanical stress induced the formation of cracks that were clearly visible in the SEM images (Figure 6F) but did not disrupt the overall particle organization. Both emergence of structural colors and a remaining organization after deposition on the solid substrate indicate that nanometer-sized particles were forming 2D polycrystalline assemblies at the LG interface. All these results show that our method for 2D organization at the LG interface was particularly efficient with silica particles because of their high density, allowing us to crystallize both micrometer- and nanometer-sized colloids.

CONCLUSIONS

We have shown that cationic surfactants induced the adsorption of anionic particles at the air–water interface at concentrations typically 10^3 smaller than their CMC. At such concentrations, the surfactant could decrease the adsorption barrier of particles at the air–water interface but did not significantly affect the charge of particles. Particles thus adsorbed with a low contact angle and remained stabilized (i.e., they did not aggregate) mostly through electrostatic repulsions operating in the water phase. We demonstrated that when the number of adsorbed particles was high enough, the combination of interparticle electrostatic repulsion and the long-range gravity-driven attraction via the collective deformation of the interface led to the formation of highly ordered polycrystalline assemblies. We showed that interparticle repulsion and long-range attraction was directly controlled by surfactant and particle concentrations, respectively, making it possible to control not only the type of organization (disordered, densely packed crystalline, densely packed amorphous, and loosely packed gel) of the 2D colloidal assemblies but also the interparticle distance.

With these findings, we have critically expanded the potential of surfactants in addressing interfacial organization, and in particular to control the behavior of particles at interfaces. Widely used to increase particle hydrophobicity or to modify interfacial energies, we have shown here that surfactants can also directly govern colloidal crystallization at the air–water interface. Demonstrated with two types of conventional cationic surfactants, two different particle types and both micrometer- and nanometer-sized colloids, we expect our strategy to be readily applicable to a wide range of surfactant/particle systems of scientific or industrial interest. We also believe that much larger colloidal assemblies can be produced. Finally, the two practical ways to prepare colloidal crystals described in this work, namely the "straight" and the "flipping" methods, can be easily adapted to various user needs. Advantageously combining extreme simplicity and controllability over the colloidal assembly characteristics (through well-defined physicochemical parameters such as surfactant or particle concentration), they concretely pave the way toward a universal and highly robust procedure for user-defined and finely tunable colloidal assemblies.

ASSOCIATED CONTENT

Supporting Information

The Supporting Information is available free of charge on the ACS Publications website at DOI: 10.1021/acs.langmuir.8b03233.

Brightfield transmission microscopy images of the LG interface for a suspension of anionic PS particles and different amounts of the negatively charged surfactant sodium dodecyl sulfate; brightfield transmission microscopy images of the LG interface for a suspension of anionic PS particles and different amounts of the neutral surfactant triethoxy monooctylether; evolution of the microstructure of the 2D colloidal assemblies obtained with the "flipping method" versus DTAB concentration; evolution of the microstructure of the 2D colloidal assemblies obtained with the "flipping method" versus particle concentration at a fixed DTAB concentration; evolution of the microstructure of the 2D colloidal assemblies obtained with the "flipping method" versus particle concentration at a fixed DTAB concentration; number of adsorbed particles at the LG interface versus DTAB concentration, at a fixed particle concentration, as obtained from the "straight method" with anionic PS particles (PDF)

Formation of the 2D crystal after loading the surfactant/particle mixture in the chamber (AVI)

Crystallization process of particles adsorbed at the LG interface (AVI)

Disordered structure with patches adopting a 2D gel-like morphology (AVI)

Fast crystallization of silica particles at the center of the LG interface (AVI)

DOI: 10.1021/acs.langmuir.8b03233
Langmuir 2018, 34, 15526–15536

AUTHOR INFORMATION

Corresponding Authors

*E-mail: anyfas.com@gmail.com (M.A.).
*E-mail: damien.baigl@ens.fr (D.B.).

ORCID

Manos Anyfantakis: 0000-0002-4572-5641
Hans-Jürgen Butt: 0000-0001-5391-2618
Bernard P. Binks: 0000-0003-3639-8041
Damien Baigl: 0000-0003-1772-3080

Author Contributions

#M.A. and J.V. contributed equally to the work.

Notes

The authors declare no competing financial interest.

ACKNOWLEDGMENTS

The authors would like to thank Benoit Loppinet for his insightful suggestion of using confocal microscopy to measure the contact angle of microparticles at the air−water interface. This work was supported by the Mairie de Paris (Emergence(s) 2012) and the French Academy of Science (Subvention scientifique Del Duca 2016). This work was performed in part in the technology platform of the Institut Pierre-Gilles de Gennes (IPGG) with support from "Investissements d'Avenir" for Labex and Equipex IPGG (ANR-10-LABX-31 and ANR-10-IDEX-0001-02-PSL). M.A. acknowledges funding from the European Commission (FP7-PEOPLE-2013-IEF/project 624806 "DIOPTRA").

REFERENCES

(1) McGorty, R.; Fung, J.; Kaz, D.; Manoharan, V. N. Colloidal Self-Assembly at an Interface. *Mater. Today* **2010**, *13*, 34−42.
(2) Velev, O. D.; Gupta, S. Materials Fabricated by Micro- and Nanoparticle Assembly - The Challenging Path from Science to Engineering. *Adv. Mater.* **2009**, *21*, 1897−1905.
(3) Vogel, N.; Retsch, M.; Fustin, C.-A.; del Campo, A.; Jonas, U. Advances in Colloidal Assembly: The Design of Structure and Hierarchy in Two and Three Dimensions. *Chem. Rev.* **2015**, *115*, 6265−6311.
(4) Pieranski, P. Two-Dimensional Interfacial Colloidal Crystals. *Phys. Rev. Lett.* **1980**, *45*, 569−572.
(5) Onoda, G. Y. Direct Observation of Two-Dimensional, Dynamic Clustering and Ordering with Colloids. *Phys. Rev. Lett.* **1985**, *55*, 226−229.
(6) Denkov, N. D.; Velev, O. D.; Kralchevsky, P. A.; Ivanov, I. B.; Yoshimura, H.; Nagayama, K. Two-Dimensional Crystallization. *Nature* **1993**, *361*, 26.
(7) Zahn, K.; Méndez-Alcaraz, J. M.; Maret, G. Hydrodynamic Interactions May Enhance the Self-Diffusion of Colloidal Particles. *Phys. Rev. Lett.* **1997**, *79*, 175−178.
(8) Cavallaro, M.; Botto, L.; Lewandowski, E. P.; Wang, M.; Stebe, K. J. Curvature-Driven Capillary Migration and Assembly of Rod-like Particles. *Proc. Natl. Acad. Sci. U.S.A.* **2011**, *108*, 20923−20928.
(9) Ershov, D.; Sprakel, J.; Appel, J.; Cohen Stuart, M. A.; van der Gucht, J. Capillarity-Induced Ordering of Spherical Colloids on an Interface with Anisotropic Curvature. *Proc. Natl. Acad. Sci. U.S.A.* **2013**, *110*, 9220−9224.
(10) Boniello, G.; Blanc, C.; Fedorenko, D.; Medfai, M.; Mbarek, N. B.; In, M.; Gross, M.; Stocco, A.; Nobili, M. Brownian Diffusion of a Partially Wetted Colloid. *Nat. Mater.* **2015**, *14*, 908−911.
(11) Poulichet, V.; Garbin, V. Ultrafast Desorption of Colloidal Particles from Fluid Interfaces. *Proc. Natl. Acad. Sci. U.S.A.* **2015**, *112*, 5932−5937.
(12) Lenis, J.; Razavi, S.; Cao, K. D.; Lin, B.; Lee, K. Y. C.; Tu, R. S.; Kretzschmar, I. Mechanical Stability of Polystyrene and Janus Particle Monolayers at the Air/Water Interface. *J. Am. Chem. Soc.* **2015**, *137*, 15370−15373.
(13) Rey, M.; Law, A. D.; Buzza, D. M. A.; Vogel, N. Anisotropic Self-Assembly from Isotropic Colloidal Building Blocks. *J. Am. Chem. Soc.* **2017**, *139*, 17464−17473.
(14) Grzelczak, M.; Vermant, J.; Furst, E. M.; Liz-Marzán, L. M. Directed Self-Assembly of Nanoparticles. *ACS Nano* **2010**, *4*, 3591−3605.
(15) Garbin, V.; Crocker, J. C.; Stebe, K. J. Nanoparticles at Fluid Interfaces: Exploiting Capping Ligands to Control Adsorption, Stability and Dynamics. *J. Colloid Interface Sci.* **2012**, *387*, 1−11.
(16) Edel, J. B.; Kornyshev, A. A.; Urbakh, M. Self-Assembly of Nanoparticle Arrays for Use as Mirrors, Sensors, and Antennas. *ACS Nano* **2013**, *7*, 9526−9532.
(17) Tao, A.; Sinsermsuksakul, P.; Yang, P. Tunable Plasmonic Lattices of Silver Nanocrystals. *Nat. Nanotechnol.* **2007**, *2*, 435−440.
(18) Aveyard, R.; Clint, J. H.; Nees, D.; Paunov, V. N. Compression and Structure of Monolayers of Charged Latex Particles at Air/Water and Octane/Water Interfaces. *Langmuir* **2000**, *16*, 1969−1979.
(19) Maestro, A.; Guzmán, E.; Ortega, F.; Rubio, R. G. Contact Angle of Micro- and Nanoparticles at Fluid Interfaces. *Curr. Opin. Colloid Interface Sci.* **2014**, *19*, 355−367.
(20) Maestro, A.; Guzmán, E.; Santini, E.; Ravera, F.; Liggieri, L.; Ortega, F.; Rubio, R. G. Wettability of silica nanoparticle-surfactant nanocomposite interfacial layers. *Soft Matter* **2012**, *8*, 837−843.
(21) Binks, B. P.; Kirkland, M.; Rodrigues, J. A. Origin of stabilisation of aqueous foams in nanoparticle-surfactant mixtures. *Soft Matter* **2008**, *4*, 2373.
(22) Binks, B. P.; Rodrigues, J. A. Double Inversion of Emulsions By Using Nanoparticles and a Di-Chain Surfactant. *Angew. Chem., Int. Ed.* **2007**, *46*, 5389−5392.
(23) Anyfantakis, M.; Baigl, D. Dynamic Photocontrol of the Coffee-Ring Effect with Optically Tunable Particle Stickiness. *Angew. Chem., Int. Ed.* **2014**, *53*, 14077−14081.
(24) Anyfantakis, M.; Geng, Z.; Morel, M.; Rudiuk, S.; Baigl, D. Modulation of the Coffee-Ring Effect in Particle/Surfactant Mixtures: the Importance of Particle-Interface Interactions. *Langmuir* **2015**, *31*, 4113−4120.
(25) Atkin, R.; Craig, V. S. J.; Wanless, E. J.; Biggs, S. The influence of chain length and electrolyte on the adsorption kinetics of cationic surfactants at the silica-aqueous solution interface. *J. Colloid Interface Sci.* **2003**, *266*, 236−244.
(26) Paria, S.; Khilar, K. C. A review on experimental studies of surfactant adsorption at the hydrophilic solid-water interface. *Adv. Colloid Interface Sci.* **2004**, *110*, 75−95.
(27) Tyrode, E.; Rutland, M. W.; Bain, C. D. Adsorption of CTAB on Hydrophilic Silica Studied by Linear and Nonlinear Optical Spectroscopy. *J. Am. Chem. Soc.* **2008**, *130*, 17434−17445.
(28) Velikov, K. P.; Durst, F.; Velev, O. D. Direct Observation of the Dynamics of Latex Particles Confined inside Thinning Water−Air Films. *Langmuir* **1998**, *14*, 1148−1155.
(29) Williams, D. F.; Berg, J. C. The aggregation of colloidal particles at the air-water interface. *J. Colloid Interface Sci.* **1992**, *152*, 218−229.
(30) Abdel-Fattah, A. I.; El-Genk, M. S. Sorption of Hydrophobic, Negatively Charged Microspheres onto a Stagnant Air/Water Interface. *J. Colloid Interface Sci.* **1998**, *202*, 417−429.
(31) Abdel-Fattah, A. I.; El-Genk, M. S. On colloidal particle sorption onto a stagnant air-water interface. *Adv. Colloid Interface Sci.* **1998**, *78*, 237−266.
(32) Lee, D.-G.; Cicuta, P.; Vella, D. Self-Assembly of Repulsive Interfacial Particles via Collective Sinking. *Soft Matter* **2017**, *13*, 212−221.
(33) Mohammadi, R.; Amirfazli, A. Contact Angle Measurement for Dispersed Microspheres Using Scanning Confocal Microscopy. *J. Dispersion Sci. Technol.* **2005**, *25*, 567−574.
(34) Cui, Z.-G.; Yang, L.-L.; Cui, Y.-Z.; Binks, B. P. Effects of Surfactant Structure on the Phase Inversion of Emulsions Stabilized by Mixtures of Silica Nanoparticles and Cationic Surfactant. *Langmuir* **2010**, *26*, 4717−4724.

DOI: 10.1021/acs.langmuir.8b03233
Langmuir 2018, 34, 15526−15536

(35) Mishra, H.; Enami, S.; Nielsen, R. J.; Stewart, L. A.; Hoffmann, M. R.; Goddard, W. A.; Colussi, A. J. Bronsted Basicity of the Air-Water Interface. *Proc. Natl. Acad. Sci. U.S.A.* **2012**, *109*, 18679−18683.
(36) Xu, Y.; Konrad, M. P.; Lee, W. W. Y.; Ye, Z.; Bell, S. E. J. A Method for Promoting Assembly of Metallic and Nonmetallic Nanoparticles into Interfacial Monolayer Films. *Nano Lett.* **2016**, *16*, 5255−5260.
(37) Binks, B. P. Colloidal Particles at a Range of Fluid-Fluid Interfaces. *Langmuir* **2017**, *33*, 6947−6963.

DOI: 10.1021/acs.langmuir.8b03233
Langmuir 2018, 34, 15526−15536